SIAM J. APPL. MATH.
Vol. 55, No. 5, pp. 1362–1371, October 1995

010

TIP RECONSTRUCTION FOR THE ATOMIC FORCE MICROSCOPE*

RICHARD MILLER,† JAMES VESENKA,‡ AND ERIC HENDERSON‡

Abstract. Colloidal gold particles are used as hard, spherical imaging targets to assist in the reconstruction of the three-dimensional atomic force probe geometry. The mathematical model for this reconstruction is developed, and a solution is proposed. The voracity of the probe reconstruction depends on image noise and numerical derivative approximations.

Key words. atomic force microscope, differential equation, image analysis

AMS subject classifications. 34A09, 35A40, 92B99

Introduction. The atomic force microscope (AFM) [2] is essentially a high-resolution profilometer capable of imaging surface features from specimens from the atomic scale to whole cells (six orders of magnitude). An unsolved technological problem of the AFM for imaging "rough" specimens (anything over a few nanometers in height) is that the lateral resolution of the AFM images is limited by the probe sharpness. The more dull the scanning probe is, the more distortions that appear in the image, especially for large specimens. There have been two approaches to solving this problem: making sharper probes and removing the probe contribution to the overall image through image analysis. The sharpest probes have a radius of curvature of about 5 nm [12]. This is still too large for detailed imaging of small biomolecules, such as actin filaments [8].

Even if exceptionally sharp probes can be manufactured, they tend to contaminate easily, resulting in image distortion. Efforts aimed at removing the probe contribution to AFM images [6] assume a tip geometry, usually parabolic. Rough estimates for the radius of curvature can be obtained in the case of well-defined, incompressible specimens in contact with parabolic tip geometry [9] or spherical tip geometry [10]. These are simple approximations and assume perfectly shaped probes. These assumptions can be dangerous because scanning probes tend to be asymmetric [1], [5], and asymmetries can be easily detected even for specimens only a few nanometers tall [11].

Our solution involves the use of colloidal gold particles to "reconstruct" the three-dimensional probe shape. Colloidal gold particles have been used to calibrate the vertical dimensions of the AFM, determine the proper scanning orientation during imaging, determine the damage threshold of compressible specimens, and *estimate* probe geometry [10]. From AFM images of these highly uniform, spherical colloidal gold particles we plan to reconstruct the three-dimensional probe shape to nanometer resolution. With this "tip surface function" we believe it will be possible to more accurately determine the reconstructed surface image.

The mathematical solution assumes that the sample or target, the colloidal gold particles, is spherical. We generate a three-dimensional AFM image that is a map composed of the specimen shape and probe shape, loosely called a "convolution." The usage of the term "convolution" is not to be taken literally, as other authors have

* Received by the editors September 14, 1993; accepted for publication (in revised form) October 5, 1994.

† Department of Mathematics, Iowa State University, Ames, Iowa 50011.

‡ Department of Zoology and Genetics, Iowa State University, Ames, Iowa 50011.

shown that regions of missing information cannot be restored by deconvolution [4], [6]. By extracting the known specimen shape we deduce the probe shape. We can reliably reconstruct a probe shape for any local region where probe has only one maximum and has reasonable curvature. Once the probe shape is determined the shape of a specimen imaged by the probe could be accurately determined through the reverse process. In practice colloidal gold particles can be simultaneously coabsorbed with biomolecules [10], [11], enabling the determination of the probe shape and neighboring biomolecule's shape.

Basic equations and their solution. We will assume that the sample or target is a sphere of known radius R. Since the underside of the sphere can never be probed by any tip (see Fig. 1(a)), this portion of the sample can be ignored. Hence our sample function will be taken as

$$S(X,Y) = \begin{cases} R + \sqrt{R^2 - X^2 - Y^2} & \text{for } X^2 + Y^2 \le R^2, \\ 0 & \text{for } X^2 + Y^2 > R^2. \end{cases} \tag{1}$$

We assume that the tip has a smooth surface with a single minimum. Note that a tip region with more than one local minimum can often be divided into two or more regions, each of which has a single minimum. We assume that the tip will always contact the target ball at exactly one point. These assumptions can be given precise form as follows: There is a smooth function $T(x,y)$ which describes the surface of the tip. The function T has a minimum at $x = y = 0$; otherwise its gradient is not zero, i.e., $(T_x, T_y) \neq (0,0)$. For any point (x,y) and any φ, the curvature of the curve $z(t) \triangleq T(x + t\cos\varphi, y + t\sin\varphi)$ is larger than $-1/R$ at $t = 0$.

Spherical, elliptical, or parabolic tips of reasonable curvature always satisfy these assumptions. The finite width of the tip always causes tip distortion. When the sample is scanned, the image I will be positive before the tip is over the target; see Fig. 1.

Similar widening of the image will occur on all sides of the sample. Suppose the ball is located at the point $(0,0)$ on the scan grid. If the minimum point of the tip is located at scan position (σ_1, σ_2) (see Fig. 1(b)), then the tip and the sample will make contact at a point located at (x,y) in tip coordinates and (X,Y) in sample coordinates. From Fig. 1(b) we see that

$$\sigma_1 + x = X, \qquad \sigma_2 + y = Y, \tag{2.a}$$

and from Fig. 1(a)

$$I(\sigma_1, \sigma_2) + T(x,y) = S(X,Y). \tag{2.b}$$

Since the tip and sample must make tangential contact, it is also true that

$$\frac{\partial T}{\partial x} = \frac{\partial S}{\partial X}, \qquad \frac{\partial T}{\partial y} = \frac{\partial S}{\partial Y}; \tag{3}$$

i.e.,

$$\frac{\partial T}{\partial x}(x,y) = \frac{\partial S}{\partial X}(\sigma_1 + x, \sigma_2 + y), \qquad \frac{\partial T}{\partial y}(x,y) = \frac{\partial S}{\partial Y}(\sigma_1 + x, \sigma_2 + y).$$

From this point on the variables (x,y) will be restricted to a region where the tip satisfies our assumptions as listed above. Then σ_1, σ_2, X, and Y can be considered

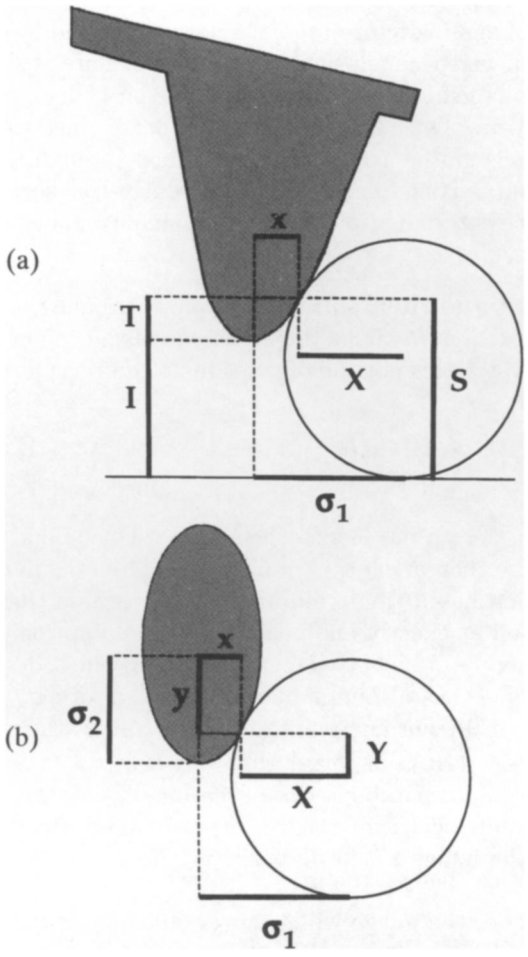

FIG. 1. (a) *Side view;* (b) *top view.*

functions of (x, y), and the image I a function of the scan variables (σ_1, σ_2). We shall use the notation

$$I_1 = \frac{\partial I}{\partial \sigma_1}, \quad I_2 = \frac{\partial I}{\partial \sigma_2}, \quad S_1 = \frac{\partial S}{\partial X}, \quad S_{12} = \frac{\partial^2 S}{\partial X \partial Y},$$

and so on. We take partial derivations with respect to x and y in (2.b) to get

$$\begin{aligned} I_1 \frac{\partial \sigma_1}{\partial x} + I_2 \frac{\partial \sigma_2}{\partial x} + T_1 &= S_1 \left(\frac{\partial \sigma_1}{\partial x} + 1 \right) + S_2 \frac{\partial \sigma_2}{\partial x}, \\ I_1 \frac{\partial \sigma_1}{\partial y} + I_2 \frac{\partial \sigma_2}{\partial y} + T_2 &= S_1 \frac{\partial \sigma_1}{\partial y} + S_2 \left(\frac{\partial \sigma_2}{\partial y} + 1 \right). \end{aligned} \tag{4}$$

Use (3) to cancel terms in (4). Then rearrange to obtain

$$\begin{pmatrix} \frac{\partial \sigma_1}{\partial x} & \frac{\partial \sigma_2}{\partial x} \\ \frac{\partial \sigma_1}{\partial y} & \frac{\partial \sigma_2}{\partial y} \end{pmatrix} \begin{pmatrix} I_1 - S_1 \\ I_2 - S_2 \end{pmatrix} = \begin{pmatrix} 0 \\ 0 \end{pmatrix}.$$

We will see later that the matrix above is nonsingular. Hence $I_1 = S_1$ and $I_2 = S_2$, i.e.,

$$\frac{\partial I}{\partial \sigma_1}(\sigma_1, \sigma_2) - \frac{\partial S}{\partial X}(\sigma_1 + x, \sigma_2 + y) = 0, \quad \frac{\partial I}{\partial \sigma_2}(\sigma_1, \sigma_2) - \frac{\partial S}{\partial Y}(\sigma_1 + x, \sigma_2 + y) = 0. \tag{5}$$

It will turn out that (5) is the key set of equations to solve. Indeed, the following result is true.

THEOREM 1. *Suppose that the following assumption is true:*
(A) $S(X, Y)$ and $I(\sigma_1, \sigma_2)$ are given C^2 functions defined in neighborhoods of $X = Y = 0$ and $\sigma_1 = \sigma_2 = 0$ with

$$\det \begin{pmatrix} S_{11}(X, Y) & S_{12}(X, Y) \\ S_{12}(X, Y) & S_{22}(X, Y) \end{pmatrix} \neq 0 \tag{6}$$

near $X = Y = 0$.
If also

$$\det \begin{pmatrix} I_{11}(\sigma_1, \sigma_2) - S_{11}(X, Y) & I_{12}(\sigma_1, \sigma_2) - S_{12}(X, Y) \\ I_{12}(\sigma_1, \sigma_2) - S_{12}(X, Y) & I_{22}(\sigma_1, \sigma_2) - S_{22}(X, Y) \end{pmatrix} \neq 0 \tag{7}$$

near $\sigma_1 = \sigma_2 = 0, X = Y = 0$, and if $\sigma_1, \sigma_2 = 0$ is a critical point of I and $X = Y = 0$ is a critical point of S, then the problem

$$\begin{aligned} &X = x + \sigma_1, \quad Y = y + \sigma_2, \quad S(X, Y) = I(\sigma_1, \sigma_2) + T(x, y), \\ &T_x = S_X = I_{\sigma_1}, \qquad T_y = S_Y = I_{\sigma_2}, \\ &\sigma_1 = \sigma_2 = 0 \text{ at } x = y = 0 \end{aligned}$$

has a unique solution $\sigma_1(x, y), \sigma_2(x, y)$ and $T(x, y)$ for (x, y) near $(0, 0)$.

Proof. First notice that $X = \sigma_1 + x$ and $Y = \sigma_2 + y$ will be known once σ_1 and σ_2 are known. Also notice that by the implicit function theorem (5) has a smooth local solution for σ_1 and σ_2 in terms of (x, y) since the Jacobian of (5) is not zero at $\sigma_1 = \sigma_2 = x = y = 0$ by assumption (7). Also by assumption $\sigma_1 = \sigma_2 = x = y = 0$ solves (5). Hence (5) has a local solution (which must be the unique solution of (5) with zero initial conditions).

Define a function T by

$$T(x, y) = S(\sigma_1(x, y) + x, \sigma_2(x, y) + y) - I(\sigma_1(x, y), \sigma_2(x, y)).$$

Then near $x = y = 0$

$$\begin{aligned} \frac{\partial T}{\partial x} &= S_1\left(\frac{\partial \sigma_1}{\partial x} + 1\right) + S_2\left(\frac{\partial \sigma_2}{\partial x}\right) - I_1 \frac{\partial \sigma_1}{\partial x} - I_2 \frac{\partial \sigma_2}{\partial x} \\ &= S_1 + \frac{\partial \sigma_1}{\partial x}(S_1 - I_1) + \frac{\partial \sigma_2}{\partial x}(S_2 - I_2) = S_1 \end{aligned}$$

and $\partial T / \partial y = S_2$ by a similar calculation. Thus $T(x, y)$ solves

$$\begin{aligned} T_x &= S_X(\sigma_1(x, y) + x, \sigma_2(x, y) + y), \\ T_y &= S_X(\sigma_1(x, y) + x, \sigma_2(x, y) + y), \\ T(0, 0) &= 0. \end{aligned}$$

But the solution of the problem is unique. Indeed, all of the first partial derivatives of $T(x, y)$ are known continuous functions. This fixes $T(x, y)$ up to a constant. Since $T(0, 0) = 0$ is also fixed, then T is uniquely determined. □

Remark. Note that the earlier assumptions on the tip function are just a way to ensure that (7) is true. Similarly, assumption (1) implies that

$$\det \begin{pmatrix} S_{11}(X,Y) & S_{12}(X,Y) \\ S_{12}(X,Y) & S_{22}(X,Y) \end{pmatrix} = \frac{R^2}{(R^2 - X^2 - Y^2)^2} \neq 0$$

for $X^2 + Y^2 < R^2$. Hence, (6) is true near $X = Y = 0$.

Theorem 1 has a partial converse.

THEOREM 2. *If assumption* (6) *is true and if* $\sigma_1(x,y)$ *and* $\sigma_2(x,y)$ *is a smooth set of solutions of* (5) *near* $x = y = 0$ *with* $\sigma_1(0,0) = \sigma_2(0,0) = 0$, *then* (7) *must be true near* $x = y = X = Y = 0$. *Moreover, near* $x = y = 0$ *it must be true that*

$$\det \begin{pmatrix} \dfrac{\partial \sigma_1}{\partial x} & \dfrac{\partial \sigma_2}{\partial x} \\ \dfrac{\partial \sigma_1}{\partial y} & \dfrac{\partial \sigma_2}{\partial y} \end{pmatrix} \neq 0.$$

Proof. Take partial derivatives with respect to x and with respect to y in each equation in (5). The result is

$$\begin{pmatrix} I_{11} & I_{12} \\ I_{21} & I_{22} \end{pmatrix} \begin{pmatrix} \dfrac{\partial \sigma_1}{\partial x} & \dfrac{\partial \sigma_1}{\partial y} \\ \dfrac{\partial \sigma_2}{\partial x} & \dfrac{\partial \sigma_2}{\partial y} \end{pmatrix} = \begin{pmatrix} S_{11} & S_{12} \\ S_{21} & S_{22} \end{pmatrix} \begin{pmatrix} \dfrac{\partial \sigma_1}{\partial x} & \dfrac{\partial \sigma_1}{\partial y} \\ \dfrac{\partial \sigma_2}{\partial x} & \dfrac{\partial \sigma_2}{\partial y} \end{pmatrix} + \begin{pmatrix} S_{11} & S_{12} \\ S_{12} & S_{22} \end{pmatrix},$$

so that

$$\begin{pmatrix} I_{11} - S_{11} & I_{12} - S_{12} \\ I_{21} - S_{21} & I_{22} - S_{22} \end{pmatrix} \begin{pmatrix} \dfrac{\partial \sigma_1}{\partial x} & \dfrac{\partial \sigma_1}{\partial y} \\ \dfrac{\partial \sigma_2}{\partial x} & \dfrac{\partial \sigma_2}{\partial y} \end{pmatrix} = \begin{pmatrix} S_{11} & S_{12} \\ S_{12} & S_{22} \end{pmatrix}. \tag{8}$$

From assumption (6) it follows that the matrix on the right is nonsingular. Hence, each matrix in the product on the left in (8) must be nonsingular. □

Deconvolution of AFM image data taken with a known tip. If the tip shape function $T(x,y)$ is known, then tip shape can be deconvolved from image data for an unknown sample. This technique is similar to the technique outlined above for tip shape reconstruction given a known sample.

We assume that the tip function $T(x,y)$ is known. We further assume that the sample has a smooth surface $S(X,Y)$, that the sample has exactly one maximum and that the curvature of the sample allows the tip and sample always to touch at just one point. As before, at any point of contact

$$-\sigma_1 + X = x, \quad -\sigma_2 + Y = y, \tag{9.a}$$

$$-I(\sigma_1, \sigma_2) + S(X,Y) = T(x,y), \tag{9.b}$$

$$\frac{\partial S}{\partial X} = \frac{\partial T}{\partial x}, \quad \frac{\partial S}{\partial Y} = \frac{\partial T}{\partial y}. \tag{9.c}$$

This is almost the same set of equations as derived earlier with the roles of S and T reversed. We think of σ_1, σ_2, x, and y as functions of X and Y, and we differentiate

line (9.b) with respect to X and then Y:

$$-I_1\frac{\partial\sigma_1}{\partial X}-I_2\frac{\partial\sigma_2}{\partial X}+S_1=T_1\left(1-\frac{\partial\sigma_1}{\partial X}\right)-T_2\frac{\partial\sigma_2}{\partial X},$$
$$-I_1\frac{\partial\sigma_1}{\partial Y}-I_2\frac{\partial\sigma_2}{\partial Y}+S_2=T_1\left(\frac{-\partial\sigma_1}{\partial Y}\right)+T_2\left(1-\frac{\partial\sigma_2}{\partial Y}\right).$$

This and (9.c) imply that

$$\begin{pmatrix}\dfrac{\partial\sigma_1}{\partial X} & \dfrac{\partial\sigma_1}{\partial Y}\\ \dfrac{\partial\sigma_2}{\partial X} & \dfrac{\partial\sigma_2}{\partial Y}\end{pmatrix}\begin{pmatrix}I_1-T_1\\ I_2-T_2\end{pmatrix}=\begin{pmatrix}0\\0\end{pmatrix}. \tag{10}$$

Under the plausible assumption that the matrix (10) is nonsingular, it follows that $I_1=T_1$ and $I_2=T_2$, i.e.,

$$\frac{\partial I}{\partial\sigma_1}=\frac{\partial T}{\partial x},\qquad \frac{\partial I}{\partial\sigma_2}=\frac{\partial T}{\partial y}. \tag{11}$$

Equation (11) and the initial conditions

$$\sigma_1=\sigma_2=0,\quad I=0,\quad X=Y=0$$

mean that $S(X,Y)$ can be determined by the same type of analysis as used in the last section; i.e., the existence and uniqueness for the deconvolution problem are similar to those already done for the reconstruction of the tip from a known sample.

Numerical solutions. The existence and uniqueness results of the next-to-last section show that the key to finding the tip function $T(x,y)$ is to first solve the nonlinear system of equation (5) for σ_1 and σ_2 as functions of (x,y). For reasons that will be explained later, standard solution schemes such as Newton's method could not be made to work. Our solution method was to reduce (5) to an initial value problem for a system of partial differential equations. This system of differential equations was integrated to find $\sigma_1(x,y)$ and $\sigma_2(x,y)$. The desired system of partial differential equations follows immediately from (8):

$$\begin{pmatrix}\dfrac{\partial\sigma_1}{\partial x} & \dfrac{\partial\sigma_1}{\partial y}\\ \dfrac{\partial\sigma_2}{\partial x} & \dfrac{\partial\sigma_2}{\partial y}\end{pmatrix}=\begin{pmatrix}I_{11}-S_{11} & I_{12}-S_{12}\\ I_{12}-S_{12} & I_{22}-S_{22}\end{pmatrix}^{-1}\begin{pmatrix}S_{11} & S_{12}\\ S_{12} & S_{22}\end{pmatrix}. \tag{12}$$

Since partial derivatives of S can be computed using (1), the final result is

$$\begin{pmatrix}\dfrac{\partial\sigma_1}{\partial x} & \dfrac{\partial\sigma_1}{\partial y}\\ \dfrac{\partial\sigma_2}{\partial x} & \dfrac{\partial\sigma_2}{\partial y}\end{pmatrix}$$
$$=\begin{pmatrix}I_{11}\alpha^3-Y^2+R^2 & I_{12}\alpha^3+XY\\ I_{12}\alpha^3+XY & I_{22}\alpha^3-X^2+R^2\end{pmatrix}^{-1}\begin{pmatrix}Y^2-R^2 & -XY\\ -XY & X^2-R^2\end{pmatrix}, \tag{13.a}$$

$$\frac{\partial T}{\partial x}=-\frac{X}{\alpha},\quad \frac{\partial T}{\partial y}=-\frac{Y}{\alpha}, \tag{13.b}$$

where

$$X = \sigma_1 + x, \quad Y = \sigma_1 + y, \quad \alpha = \sqrt{R^2 - X^2 - Y^2}. \tag{13.c}$$

From Fig. 1(b) it follows that when the low point on the tip touches the high point on the sample, all variables are zero, i.e.,

$$x = y = 0, \quad \sigma_1 = \sigma_2 = 0, \quad I = 0. \tag{14}$$

Equation (13) and initial conditions (14) are sufficient to determine the shape function $T(x, y)$ of any single-minimum piece of the tip once the scan data $I(\sigma_1, \sigma_2)$ is known. Indeed, if $I(\sigma_1, \sigma_2)$ is known, then all second derivatives I_{ij} will be known. Hence (13.a) and (13.c) imply that σ_1 and σ_2 satisfy a system of equations of the form

$$\begin{pmatrix} \dfrac{\partial \sigma_1}{\partial x} \\ \dfrac{\partial \sigma_2}{\partial x} \end{pmatrix} = \begin{pmatrix} g_{11}(x, y, \sigma_1, \sigma_2) \\ g_{12}(x, y, \sigma_1, \sigma_2) \end{pmatrix}.$$

In particular $\sigma_1(0, 0) = \sigma_2(0, 0) = 0$ and

$$\begin{pmatrix} \dfrac{\partial \sigma_1}{\partial x}(x, 0) \\ \dfrac{\partial \sigma_2}{\partial x}(x, 0) \end{pmatrix} = \begin{pmatrix} g_{11}(x, 0, \sigma_1(x, 0), \sigma_2(x, 0) \\ g_{12}(x, 0, \sigma_1(x, 0), \sigma_2(x, 0) \end{pmatrix}.$$

This is a nonlinear system of ordinary differential equations which can be solved for $\sigma_1(x, 0)$ and $\sigma_2(x, 0)$ for $x > 0$ and then separately solved for $x < 0$.

Similarly from (13.a) and (13.c) we see that for any fixed x, σ_1, and σ_2 satisfy equations of the form

$$\begin{pmatrix} \dfrac{\partial \sigma_1}{\partial y}(x, y) \\ \dfrac{\partial \sigma_2}{\partial y}(x, y) \end{pmatrix} = \begin{pmatrix} g_{21}(x, y, \sigma_1, \sigma_2) \\ g_{22}(x, y, \sigma_1, \sigma_2) \end{pmatrix}.$$

This system of nonlinear ordinary differential equations can be solved for $\sigma_1(x, y)$ and $\sigma_2(x, y)$ for $y > 0$ or for $y < 0$ whenever $\sigma_1(x, 0)$ and $\sigma_2(x, 0)$ are known. Thus we can compute σ_1 and σ_2 at all points on a grid.

Clearly a variety of rectangular paths can be chosen to integrate σ_1 and σ_2 from $(0, 0)$ to any (x, y). Once σ_1 and σ_2 are known, then $T(x, y)$ is determined by integrating (13.b) or directly from the relation

$$T(x, y) = S(x + \sigma_1(x, y), y + \sigma_2(x, y)) - I(\sigma_1(x, y), \sigma_2(x, y)).$$

Note that if this scheme is to work, then the inverse matrix in (13.a) must exist. The existence of this inverse follows from assumption (7) in Theorem 1. A more serious problem is that the image function $I(\sigma_1, \sigma_2)$ is known only as data—noisy data—and is known only at grid points. Derivatives of I can be estimated at grid points in a standard way by fitting locally smooth approximate functions and differentiating the approximations. Interpolation can be used to estimate the derivatives of $I(\sigma_1, \sigma_2)$ at nongrid points. All of this must be done carefully. However, it is possible to obtain satisfactory approximations using orthodox techniques in the case where the tip is not nearly flat in the x or the y direction near its minimum. The approximations so obtained are sufficiently accurate to use in an integration scheme but could not

be made accurate enough to use in a Newton or modified Newton scheme for the nonlinear system (5).

We remark that our numerical scheme will compute not only $T(x, y)$ at grid points but also $\frac{\partial T}{\partial x}$ and $\frac{\partial T}{\partial y}$ since, e.g.,

$$\frac{\partial T}{\partial x} = \frac{\partial S}{\partial X} = -\frac{X}{\sqrt{R^2 - X^2 - Y^2}} = -\frac{\sigma_1 + x}{\sqrt{R^2 - (x + \sigma_1)^2 - (y + \sigma_2)^2}}.$$

Similarly, second derivatives of T can be computed, e.g.,

$$\begin{aligned}\frac{\partial^2 T}{\partial x^2} &= \frac{\partial}{\partial x}\left(\frac{\partial S}{\partial X}\right) = \frac{\partial^2 S}{\partial X^2}\frac{\partial X}{\partial x} + \frac{\partial^2 S}{\partial Y \partial X}\frac{\partial Y}{\partial x} \\ &= \frac{Y^2 - R^2}{(\sqrt{R^2 - X^2 - Y^2})^3}\left(\frac{\partial \sigma_1}{\partial x} + 1\right) - \frac{XY}{(\sqrt{R^2 - X^2 - Y^2})^3}\frac{\partial \sigma_2}{\partial x}.\end{aligned}$$

The values of all first and second derivatives of T will be needed for the deconvolution algorithm outlined in the following paragraph. All of these derivatives can be computed and saved as $T(x, y)$ is being computed.

Once T is known, its shape can be used when deconvolving images of unknown samples. Notice that not only $T(x, y)$ but also its first and second derivatives are needed in order to compute the unknown sample shape function $S(X, Y)$. If the analytic form for $T(x, y)$ is known or can be estimated, then these derivatives can be computed from the analytic form. If $T(x, y)$ was found by using the algorithm described in the last section, then these derivatives can be computed along with $T(x, y)$. The derivatives of $I(\sigma_1, \sigma_2)$ must be estimated from the image data as before.

Conclusions. We have developed a simple mathematical description of AFM tip shape which does not depend on any a priori model of the tip. We are now in the process of reducing this description to computer code. We plan to compare our numerical results for oxide tips and for electron beam–deposited tips with electron microscope (TEM) images of such tips. Figure 2(a) shows data $I(\sigma_1, \sigma_2)$ for an electron beam–deposited tip. Figure 2(b) shows the three-dimensional reconstruction of the tip. In Fig. 2(c) the $y = 0$ profile of this reconstruction is superimposed over a TEM image of this tip. Agreement is seen to be good to within a nanometer except near the edge of the reconstruction. The edge errors are thought to be caused mainly by our inability to accurately estimate first and second derivatives of $I(\sigma_1, \sigma_2)$ near the edges of scan. Note also that the reconstructed "cap" is not symmetric; that is, it goes up one side of the tip more than the other. This is because tips are tilted by approximately 10° during acquisition of the data. Hence the region which can be reconstructed is not symmetric.

The main mathematical sources of error are all related to making the appropriate numerical approximations of first- and second-order derivatives from the raw AFM images. These lead to errors up the sides of the tip, a region of the tip that also provides some difficulty in terms of experimental results. All oxide tips examined so far have either multiple local minimum and/or very blunt tips. We have not yet been able to reconstruct such a tip.

There are several experimental sources of error that can lead to erroneous tip reconstruction. "Roundness" of the colloidal gold particles and residual substrate preparation media surrounding the gold are the two greatest problems. These impair the principle assumption of an ideal spherical target that the tip reconstruction is based upon. Colloidal gold particles can be manufactured routinely between 10 and 20 nm

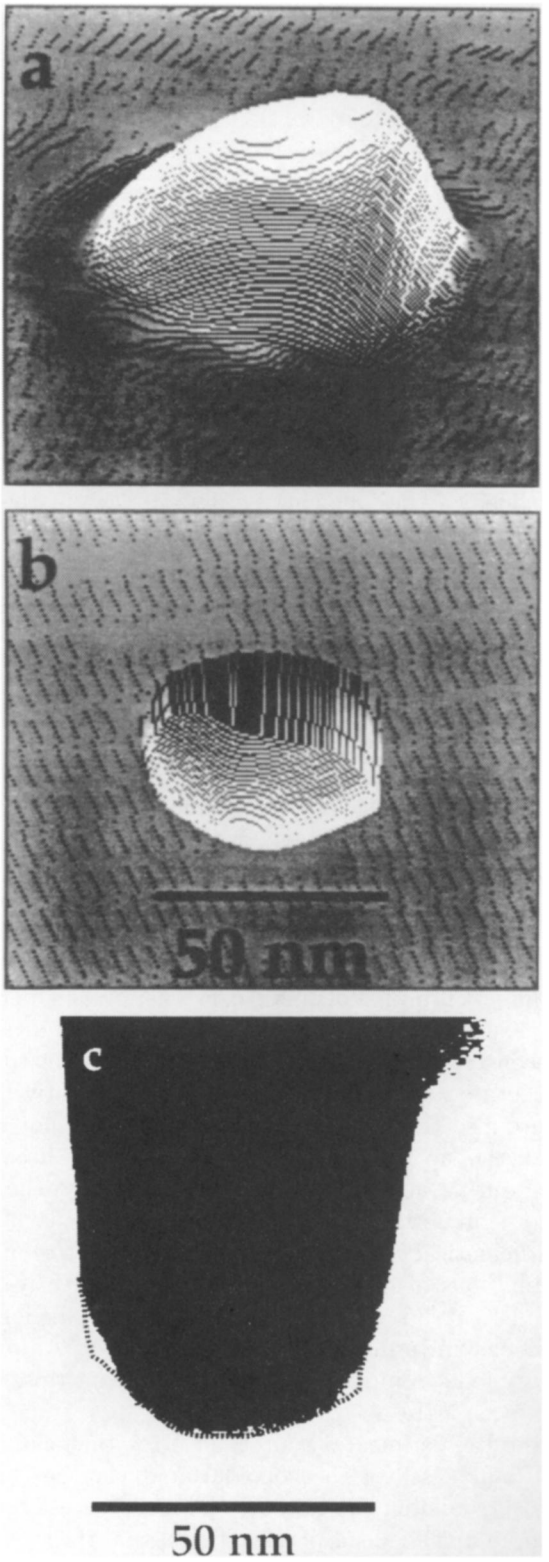

FIG. 2. (a) *Data for an electron beam–deposited tip;* (b) *reconstruction of the tip;* (c) *TEM image of the tip.*

radius of curvature but tend to be asymmetric above 20 nm in diameter [10]. Still, a reasonable fraction of the larger particles are symmetric under electron microscopic analysis.

The problem of substrate preparation residue surrounding the colloidal gold is more subtle. The residue can be seen to surround the base from colloidal gold particles that have been pushed off the surface. The remaining "pedestal" is typically about 1–2 nanometers tall at the edges. For intact gold particles, imaging any portion of this pedestal corresponds to the reconstructed portion of the tip farthest from the apex. This is in an area that is mathematically unreliable and must be ignored when employed for the reconstruction of the AFM sample. This portion of the probe also corresponds to the edge region of the sample, a region containing unknown sample information that is not possible to reconstruct [4], [6].

REFERENCES

[1] M. J. Allen, N. V. Hud, M. Balooch, R. J. Tench, W. J. Siekhaus, and R. Balhorn, *Tip–radius–induced artifacts in AFM images of protamine-complexed DNA fibers*, Ultramicroscopy, 42–44 (1992), pp. 1095–1096.

[2] G. Binning, C. F. Quate, and Ch. Gerber, *Atomic force microscope*, Phys. Rev. Lett., 56 (1986), pp. 930–933.

[3] J. E. Griffith, D. A. Grigg, M. J. Vasile, P. E. Russell, and E. A. Fitzgerald, *Characterization of scanning probe microscope tips for line width measurement*, J. Vac. Sci. Technol., B 9 (1991), pp. 3586–3589.

[4] D. A. Grigg, P. E. Russell, J. E. Griffith, M. J. Vasile, and E. A. Fitzgerald, *Probe characterization for scanning probe metrology*, Ultramicroscopy, 42–44 (1992), pp. 1616–1620.

[5] P. Grütter, W. Zimmermann-Edling, and D. Brodbeck, *Tip artifacts of microfabricated force sensors for atomic force microscopy*, Appl. Phys. Lett., 60 (1992), pp. 2741–2743.

[6] D. Keller, *Reconstruction of STM and AFM images distorted by finite tip size*, Surface Science, 253 (1992), pp. 353–365.

[7] D. Keller and C. Chih-Chung, *Imaging steep high structures by scanning force microscopy with election beam deposited tips*, Surface Science, 268 (1992), pp. 333–339.

[8] D. Keller and F. S. Franke, *Envelope reconstruction of probe microscope images*, Surface Science, 294 (1993), pp. 409–419.

[9] T. Thundat, X.-Y. Zheng, S. L. Sharp, D. P. Allison, R. J. Warmack, D. C. Joy, and T. L. Ferrell, *Calibration of atomic force microscope tips using biomolecules*, Scanning, 6 (1992), pp. 903–910.

[10] J. Vesenka, S. Manne, R. Giberson, T. Marsh, and E. Henderson, *Colloidal gold particles as an incompressible atomic force microscope imaging standard for assessing the compressibility of biomolecules*, Biophysical J., 56 (1993), pp. 992–997.

[11] J. Vesenka, S. Manne, G. Yang, C. J. Bustamante and E. Henderson, *Humidity effects on atomic force microscopy of gold–labeled DNA on mica*, Scanning, 7 (1993), pp. 781–788.

[12] H. Ximen and P. E. Russell, *Microfabrication of AFM tips using focused ion and electron beam techniques*, Ultramicroscopy, 42–44 (1992), pp. 1526–1532.